THE JOURNAL OF PHYSICAL CHEMISTRY C

Article

Cite This: J. Phys. Chem. C 2019, 123, 29394−29407

pubs.acs.org/JPCC

Alcoholic Solvent Influence on ZnO Synthesis: A Joint Experimental and Theoretical Study

Ankica Šarić,*[,†] Ines Despotović,[‡] and Goran Štefanić[†]

[†]Division of Materials Physics, Centre of Excellence for Advanced Materials and Sensing Devices, Ruđer Bošković Institute, Bijenička 54, HR-10002 Zagreb, Croatia

[‡]Division of Physical Chemistry, Ruđer Bošković Institute, Bijenička 54, HR-10002 Zagreb, Croatia

Supporting Information

ABSTRACT: Zinc oxide nanoparticles were prepared by a solvothermal synthesis using various alcoholic reaction solvents including ethanol, 1-propanol, 1-butanol, 1-pentanol, and 1-octanol, at 170 °C. The nucleation and growth processes of the ZnO nanoparticles were investigated by X-ray diffraction (XRD) and field emission scanning electron microscopy (FE-SEM) characterization, and they were corroborated by means of quantum chemical calculations at the density functional theory level (DFT). On the basis of the results of joint microstructural and theoretical study, the nucleation and preferential growth mechanism of ZnO nanoparticles is proposed. The effect of various alcoholic solvent on the overall shape and growth rate along the preferential *c*-axis of ZnO nanoparticles were corroborated by means of theoretical simulations of interface-solvent interaction by using nanoclusters $(ZnO)_n$ (n = 12 and 36). The $(ZnO)_{36}$−$CH_3(CH_2)_nOH$ ($n \leq 7$) interaction has been found to be spontaneous exergonic process only in the presence of 1-butanol as reaction medium with $\Delta G^*_{INT} = -4.95$ kcal mol^{-1}, whereas endergonic in the presence of all remaining alcohols used ($\Delta G^*_{INT} > 0$). The results of X-ray diffraction size-strain analysis reveal that solely the use of 1-butanol as solvent leads to rather isotropic crystallite shape ($D_v \perp c$-ax ∼12 nm, $D_v \| c$-ax ∼12 nm), whereas in the presence of all remaining alcohols used ZnO nanoparticles grew prevailing in the *c*-direction to form nanorods. The alcohols of different size and polarity acts as a solvent and reactant as well as controlling agents for crystal growth, providing different binding interactions involved in both the nucleation processes and preferential growth of ZnO nanoparticles. The calculated values of $E_{O\cdots H}$ and E_{Zn-O} of $(ZnO)_{36}$−$CH_3(CH_2)_7OH$ (1-octanol) interaction indicate a weaker interaction of the nonpolar 1-octanol and polar a little positively charged Zn surface of ZnO crystal as well as a higher preferential growth rate along the *c*-axis in comparison to polar alcoholic media.

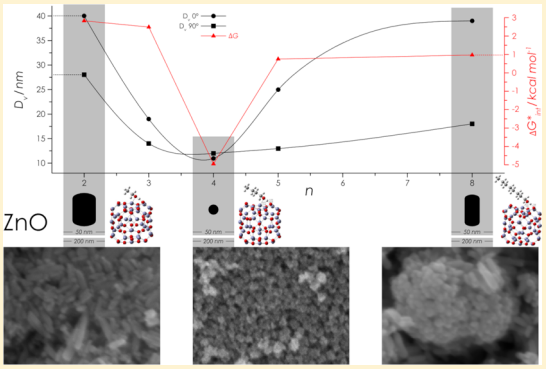

1. INTRODUCTION

Zinc oxide is of interest in many applications as a especially important material due to powerful combination of optical, electrical, microstructural, and other properties, as well as thermal and chemical stability. A direct wide band gap (3.37 eV for wurtzite ZnO) and a high exciton binding energy (60 meV) makes ZnO a multifunctional material for the fabrication of optoelectronic devices in blue and ultraviolet spectral regions, offering excellent combination of optical, electrical and microstructural properties.[1,2] Moreover, ZnO has aroused worldwide research interest due to its low toxicity, biocompatibility, and high efficiency in heterogeneous photocatalytic reaction of organic contaminants.[3,4] For same highly technical, biomedical, or photocatalytic applications, developing a size- and morphology-controlled ZnO synthesis route is of the most importance. The systematic investigation of the size- and structure-dependent activity of ZnO nanoparticles can provide a basis for the development of nanosized materials with enhanced adsorptive and photocatalytic properties suitable for the adsorption and removal of various environmental pollutants. The photocatalytic reaction occurs at the interface, which requires the effective adsorption of reactant molecules/ions on the surface of ZnO photocatalysts. As the adsorption states of specific molecules/ions are intrinsically determined by surface atomic structures of ZnO, the photocatalytic performance is strongly associated with the electronic structure and the shape of ZnO.[4−7]

So far, various shapes of ZnO nanoparticles have been prepared successfully.[8−10] Xu et al.[9] reported a facile synthesis of ZnO with different morphologies (nanospherical, nanorods, tubular, cauliflower-like, truncated hexagonal conical, and hourglasslike) via simple solvothermal method in which zinc acetylacetonate was used as the zinc source. The authors discussed the influence of the solvents on the morphology of ZnO samples as well as the effect of the morphologies on the photocatalytic activity.[9] The alcoholic solvent and intermediate

Received: August 3, 2019
Revised: November 6, 2019
Published: November 8, 2019

DOI: 10.1021/acs.jpcc.9b07411
J. Phys. Chem. C 2019, 123, 29394−29407

species obtained during the ZnO synthesis can show selectivity to the binding to different crystal facets of polar ZnO or suppress its crystal growth, which leads to preferential crystal growth.[11] In general synthesis conditions, ZnO nanostructures tend to grow along the *c*-axis. Chaudari et al.[10] reported the synthesis and formation mechanism of hollow hexagonal nanotowers. Hollow tubular ZnO structures have attracted great interest and have been recently prepared by simple hydrolysis of zinc acetylacetonate at 90 °C.[12] The Salavati-Niasari research group[13,14] discussed the influence of synthesis method on the formation and properties of ZnO nanomaterial. The physical and chemical properties, as well as the size and morphology of ZnO nanoparticles can be modified by using a different method of synthesis. ZnO nanoflowers were prepared from zinc oxalate without using additives by a fast microwave-assisted polyol method.[14] Between different synthesis routes, the solvothermal method is noted as attractive for its simplicity and the possibility to have better control of the reaction mechanism and the rate of particle growth.[15−19] Moreover, solvothermal methods can provide a facile synthesis of ZnO nanoparticles with different morphology. The basis for the new approach to obtaining ZnO nanomaterials is understanding synthesis mechanism.[16,20−23] Indeed, nonaqueous systems offer the possibility of better characterization of organic byproduct in comparison to aqueous system using conventional analytical techniques like NMR spectroscopy.[23] Nonaqueous processes can be classified as surfactant or solvent controlled. Many researchers have been focusing on the investigations of the solvent effect on the ZnO formation.[23−25] The kinetics of nucleation and ZnO nanoparticles growth are strongly dependent on the properties of solvent.[24] The development of a surfactant-free solvothermal synthesis route characterized with the presence of small number of reactants enables the deeper insight into the formation mechanism of ZnO nanoparticles and controlling the reaction pathways.[11,26,27] The alcoholic solvent and intermediate species obtained during the ZnO synthesis can show selectivity to the binding to different crystal facets of polar ZnO or suppress its crystal growth, which leads to preferential crystal growth.[11]

The synthetic efforts to obtain nanoparticles with the desired properties largely depends on the understanding of structure, crystallite size, shape, lattice defects, particles size distribution, solid solubility limits, degree of crystallinity, vibrational properties, surface layer, interaction with surrounding matrix, defects, and mechanism of electronic recombination. In previous papers,[18,19] we investigated the solvothermal synthesis of ZnO particles starting from zinc acetylacetonate and various ethanolamines as an additive in the various solvents. The strong impact of versatile family of ethanolamines as a particle growth modifier was observed. Besides, it was noted that the size and polarity of the solvent molecules had a strong influence on the size, morphology, and aggregation of primary ZnO nanoparticles during the solvothermal synthesis.

This research is a follow up to our previous combined experimental and theoretical study[17−19] and explains the mechanism of nucleation and crystal growth as dynamic balance between solvent sensitive processes. In this research, we investigated the impact of five various reaction alcoholic solvents of different size and polarity on the overall shape and growth rate along the preferential *c*-axis of ZnO nanoparticles. The aim of present joint experimental and theoretical study was to get a better insight into the mechanism of surface interactions between the ZnO nanoparticles and the molecules of alcoholic reaction solvents of different size and polarity, as well as to achieve a good control of the size and morphology of ZnO nanoparticles.

2. METHODS AND MATERIALS

Materials and Synthesis. Zinc acetylacetonate monohydrate ($Zn(C_5H_7O_2)_2{\cdot}H_2O$; *Alfa Aeser*), absolute ethanol (CH_3CH_2OH; *J. T. Baker*), 1-propanol ($CH_3(CH_2)_2OH$; *J. T. Baker*) 1-butanol ($CH_3(CH_2)_3OH$; *J. T. Baker*) 1-pentanol ($CH_3(CH_2)_4OH$; *Sigma-Aldrich*) and 1-octanol ($CH_3(CH_2)_7OH$; *Sigma-Aldrich*), all of analytical purity, were used for the preparation of samples. Commercial ZnO was provided by *Ventron*.

In a typical synthetic procedure zinc acetylacetonate monohydrate ($Zn(acac)_2{\cdot}H_2O$) in a predetermined amounts of 0.4 g were suspended in 30 mL of alcohol. Alcohols used in this research were ethanol, 1-propanol, 1-butanol, 1-pentanol, and 1-octanol. Thus, prepared transparent precursor solution was autoclaved at 170 °C for 4 h. A 50 mL Teflon-lined stainless steel autoclave was used. After autoclaving, the obtained precipitates were separated from supernatants by centrifugation, washed several times with ethanol, and dried.

Measurements and Characterization. The microstructural characterization of obtained samples was performed using a Field Emission Scanning Electron Microscope (FE-SEM) model JSM-7000F, manufactured by *Jeol Ltd.*, X-ray diffraction (XRD) by using *Italstructures* X-ray powder diffractometer (APD 2000, Cu Kα radiation, graphite monochromator, scintillation detector).

Size−Strain Line-Broadening Analysis. Size−strain line-broadening analysis of ZnO samples was performed by using the results of Le Bail refinements[28] (program GSAS[29] with a graphical user interface EXPGUI[30]) by following the procedure suggested in the size/strain round robin.[31] In the refinements, we utilized a modified pseudo-Voigt function defined by Thompson, Cox, and Hastings,[32] which gave the following expression for the observed Gaussian and Lorentzian line widths:

$$\Gamma_G^2 = U\tan^2\theta + V\tan\theta + W + P/\cos^2\theta \quad (1)$$

$$\Gamma_L = (X + X_e\cos\phi)/\cos\theta + (Y + Y_e\cos\phi)\tan\theta + Z \quad (2)$$

where θ is the Bragg angle, ϕ is the angle between the principal anisotropic broadening axis (in case of ZnO crystallites chosen to be 001) and the corresponding reciprocal lattice vector, Γ is the full width at half-maximum (fwhm) of the Gaussian (Γ_G) and Lorentzian (Γ_L) line profiles, until *U, V, W, P, X, Y, Z*, X_e, and Y_e are refinable parameters. The size and strain contribution to the line broadening can be definite by the following equations:

$$\beta_S = \lambda/(D_V\cos\theta) \quad (3)$$

$$\beta_D = e\,4\tan\theta \quad (4)$$

where λ is the wavelength, β is the integral breadth of the Voigt function resulting from size (β_S) and strain (β_D) contribution, until D_v and e present the volume-averaged domain size and the upper limits of microstrain, respectively. The values of integral breadths were gained from fwhm values by simple conversions.[31] By comparing eqs 1 and 2 with eqs 3 and 4, it was easy to recognize that parameters *X*, *P*, and X_e were related

DOI: 10.1021/acs.jpcc.9b07411
J. Phys. Chem. C 2019, 123, 29394−29407

to size broadening and Y, U, and Y_e to strain broadening. Hence, only these six profile parameters were refined in the Le Bail refinements of ZnO samples, while all other profile parameters assumed the values obtained upon refinement of the standard for which the corresponding ultrapure zincite powder (Ventron) was utilized.[33] With the intent to obtain pure physically broadened profile parameters, the values of the refined parameters were corrected by the corresponding values obtained from the standard.

Computational Details. All geometry optimization and calculations were performed by means of quantum chemical calculations at the density functional theory (DFT) level using the Gaussian 09 program (revision D1).[34] For computational efficiency, we decided to use $(ZnO)_n$ clusters used by Chen et al. with n = 12 and 36, using the polarizable solvation model.[35] The M05-2X functional[36] designed by Truhlar's group was chosen. It permits very accurate thermodynamic parameters, being specifically successful in nonbonding interactions treatment,[36−38] in particular in reproducing geometries, dipole moments, and homolytic bond energies in various zinc complexes.[39,40] The 6-31+G(d,p) + LANL2DZ mixed basis set has been used. Pople's 6-31+G(d,p) double-ξ basis set has been chosen for O and H atoms and the LANL2DZ basis (LANL2 pseudopotential for inner electrons and its associated double-ξ basis set (DZ)) was utilized for the transition-metal (Zn) atoms.[41] This gave rise to the M05-2X/6-31+G(d,p) + LANL2DZ model used for all geometry optimization, which has been frequently used for investigations of transition-metal containing systems. The geometric structures of the molecules were optimized by minimizing energies considering all geometrical parameters without imposing any molecular symmetry constraints, and by using a tight convergence condition. The Berny algorithm using redundant internal coordinates was used. Frequency calculations were made under the harmonic approximation on all the optimized structures at the same level of theory with no scaling with intent to confirm that the structures correspond to the true minima, meaning that no imaginary frequencies were present, as well as to extract thermal Gibbs free energy corrections. The final single point energies were obtained by using a highly flexible 6-311++G(2df,2pd) basis set per the O, H, and C atoms, and the same LANL2DZ ECP type basis set for zinc atoms was used. The self- consistent field (SCF) calculations were conducted under a tight condition imposing the threshold value of 10^{-8} hartree to total energy difference throughout the iteration process. The integration grid in self-consistent field calculations has been set to FineGrid having 75 radial shells and 302 angular points per shell. The 2-electron integral accuracy has been set to 10^{-13}. The FoFCou algorithm with NoSymm option was employed. All geometry optimizations, frequency calculations and single point energy evaluations has been conducted by taking solvent effects into account. To evaluate the bulk solvent effects (1-octanol, ε = 9.86; 1-pentanol, ε = 15.13; 1-butanol, ε = 17.32; 1-propanol, ε = 20.52; ethanol, ε = 24.85), the implicit SMD polarizable continuum solvation model[42] has been employed. It presents a most practical approach to simulate the solvation environment and determine the effect of the medium on the stability and structure of solutes in a solution. Starting structures were too frequently build from literature data (X-ray data), or manually sampled by using chemical intuition. In this work the latter approach was used to generate the starting structures of the ZnO−$CH_3(CH_2)_nOH$, monomers and other oligomer, $(ZnO)_{12}$−$(ZnO)_{12}$ and $(ZnO)_{36}$−$(ZnO)_{36}$ species, as well as $(ZnO)_{12}$−$CH_3(CH_2)_nOH$ and $(ZnO)_{36}$−$CH_3(CH_2)_nOH$ ($n \leq 7$). The conformational space was manually sampled for all above-mentioned structures, taking into account various donor and acceptor sites of the ZnO and alcohol molecule. The numbers of configurations were optimized, then the most stable ones were selected. Only thermodynamically the most stable structures are here reported. The interaction Gibbs free energies, ΔG^*_{INT}, are computed using the supramolecular approach according to the simple formula

$$\Delta G^*_{INT,AB} = G^*_{AB} - G^*_{A} - G^*_{B} \quad (5)$$

as the difference between the total free energy (G^*_{AB}) of the structures ZnO−$CH_3(CH_2)OH_n$, monomers or other oligomer, $(ZnO)_{12}$−$(ZnO)_{12}$ or $(ZnO)_{36}$−$(ZnO)_{36}$ species, or $(ZnO)_{12}$−$CH_3(CH_2)_nOH$ or $(ZnO)_{36}$−$CH_3(CH_2)_nOH$ ($n \leq 7$) and the sum of the total free energies ($G^*_A + G^*_B$) of the associating units A and B. The total free energy of the species in the liquid was computed using the expression

$$G^*_X = E^{Tot}_{soln} + \Delta G^*_{VRT,soln} \quad (6)$$

where the term E^{Tot}_{soln} corresponds to the basic energy of a density functional theory calculation using the SMD model, while the $\Delta G^*_{VRT,soln}$ term encompasses vibrational, rotational, and translational contribution to the solution free energy, being computed by applying the ideal gas partition functions to the frequencies calculated in the dielectric medium and the 1 M standard state. A more negative value of the binding energy implied a more stable formed species. No BSSE correction to the binding energies has been applied.

The topological analysis of the charge density distribution using the Bader's quantum theory of atoms in molecules (QTAIM)[43] is performed using AIMALL software package[44] utilizing the SMD/M05-2X/6-31+G(d,p) + LANL2DZ wave function obtained from optimization. Within the QTAIM analysis the electron density is analyzed for two major characteristics comprising of (a) the existence of critical points (CPs), which are special points where electron density exhibits a maximum, a minimum, or a saddle point in space, and (b) for the bond paths,[38] the line of maximum electron density connecting two interacting atoms in the energetic minimum structure which point out that the two atoms are bonded.[45] The point of the minimum value of electron density along that line was called the bond critical point (BCP) and the value of topological parameters, such as electron density $\rho(r_c)$, Laplacian $\nabla^2\rho(r_c)$, electronic kinetic energy $G(r_c)$, electronic potential energy density $V(r_c)$, and total energy density $H(r_c)$ at that point elucidate the features of interatomic interactions. $\nabla^2\rho(r_c) < 0$ indicates that the charge density is locally concentrated, while $\nabla^2\rho(r_c) > 0$ indicates that the charge density is locally depleted. The chemical bond nature can be described qualitatively regarding the signs and values of the electron density Laplacian $\nabla^2\rho(r_c)$ and of the electron energy density $H(r_c)$ at the corresponding bond critical point in accordance with the following criteria. The interactions characterized by $\nabla^2\rho(r_c) < 0$ and $H(r_c) < 0$ indicate a shared interaction, i.e., weakly polar and nonpolar covalent bonds. On the other hand, the interaction characterized by $\nabla^2\rho(r_c) > 0$ and $H(r_c) > 0$ points to the closed shell interactions such as weak hydrogen bonds, van der Waals interactions, and ionic bonds. The intermediate interactions which include strong hydrogen bonds and most of the coordinate bonds were

DOI: 10.1021/acs.jpcc.9b07411
J. Phys. Chem. C 2019, 123, 29394−29407

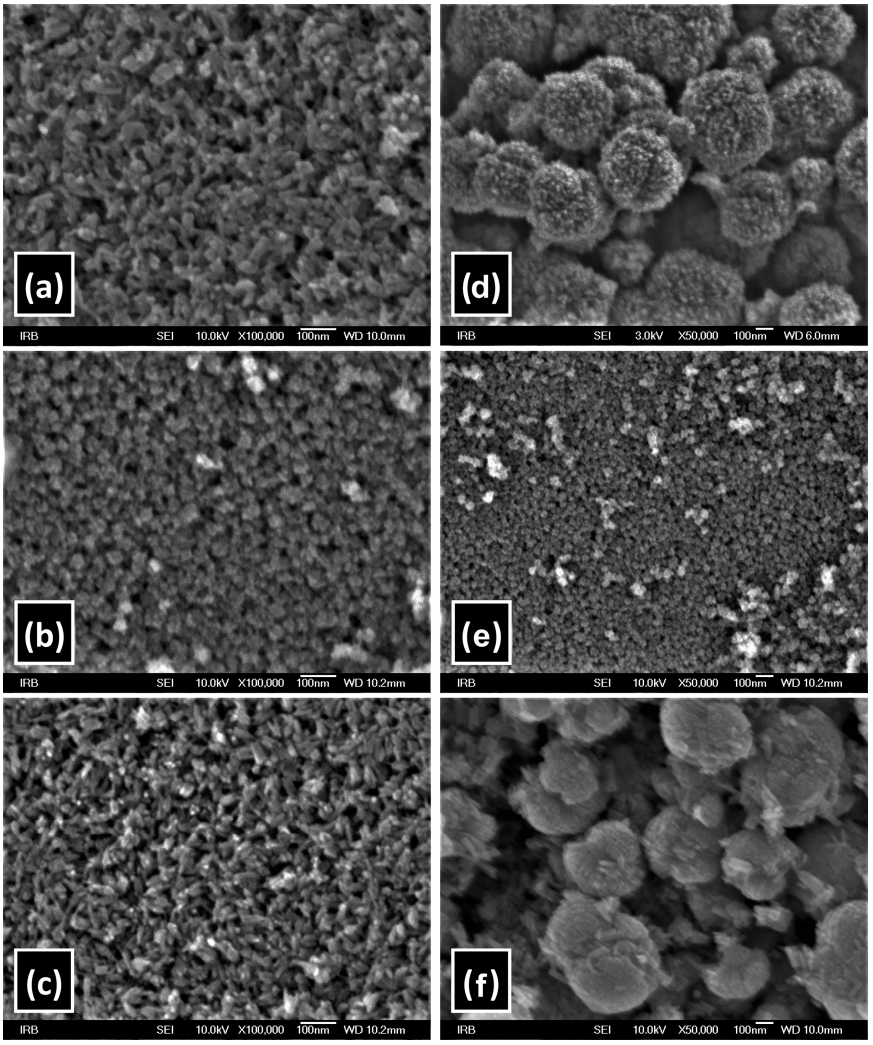

Figure 1. FE-SEM images of ZnO particles prepared at 170 °C for 4 h in (a) 1-propanol, (b, e) 1-butanol at different magnifications, (c) 1-pentanol, (d) ethanol, and (f) 1-octanol.

characterized by $\nabla^2\rho(r_c) > 0$ and $H(r_c) < 0$.[46,47] A especially high negative value of the $\nabla^2\rho(r_c)$ is an indication of a strong covalent bond, while a high positive value corresponds to a strong noncovalent bond. The energies of the Zn−O coordinate bond and of other intra- and intermolecular hydrogen bonds were calculated by Espinosa's equation

$$E = 0.5V(r_c) \tag{7}$$

where E is the bond energy (au), and $V(r_c)$ is the potential energy density (au) at the corresponding critical point.[48] Espinosa's relationship is widely employed for the energy estimation of different types of hydrogen,[49,50] van der Waals,[51] coordinate,[52,53] and homopolar bonds.[54]

3. RESULTS AND DISCUSSION

Structure and Morphology. Irrespective of the presence of various alcoholic solvent XRD analysis shows the formation of hexagonal wurtzite ZnO structure. Indeed, different ZnO crystallite sizes and different particle morphologies were obtained in the presence of alcohols of different size and polarity, including ethanol, 1-propanol, 1-butanol, 1-pentanol, and 1-octanol. The microstructures and morphologies of ZnO particles in as-prepared samples were characterized with XRD and FE-SEM Figure 1 shows the SEM images of ZnO particles prepared at 170 °C for 4 h in (a) 1-propanol, (b, e) 1-butanol at different magnifications, (c) 1-pentanol, (d) ethanol, and (f) 1-octanol.

ZnO nanoparticles prepared in 1-butanol consists of small irregular spherical aggregates <50 nm in size made up of a few loosely assembled spherical nanoparticles (~12 nm), as shown in the SEM images at different magnifications in Figure 1, parts b and e. Furthermore, it is clearly illustrated that irregular nanoparticle aggregates are loosely coupled to each other. The results obtained by FE-SEM are in agreement with those obtained by XRD (Figure 2, Table 1), suggesting that each fine spherical ZnO nanoparticle consists of a single crystallite. Alongside, the results of X-ray diffraction line-broadening analysis suggest a preferably isotropic crystallite shape in sample ZnO prepared in 1-butanol ($D_v \perp c$-ax ~ 12 nm; $D_v \| c$-ax ~ 12 nm) as shown in Figure 2c and Table 1. On the other hand, ZnO nanorods were obtained with 1-propanol, 1-pentanol, ethanol, and 1-octanol as reaction solvent, as shown in the SEM images in Figure 1a, c, d, and f.

The results of X-ray diffraction size-strain analysis indicated the presence of size anisotropy with significantly narrower diffraction lines along the direction ⟨00l⟩ in samples ZnO obtained in all above-mentioned alcohols except in the case of 1-butanol (Figure 2, Table 1). Indeed, the formation of

DOI: 10.1021/acs.jpcc.9b07411
J. Phys. Chem. C 2019, 123, 29394−29407

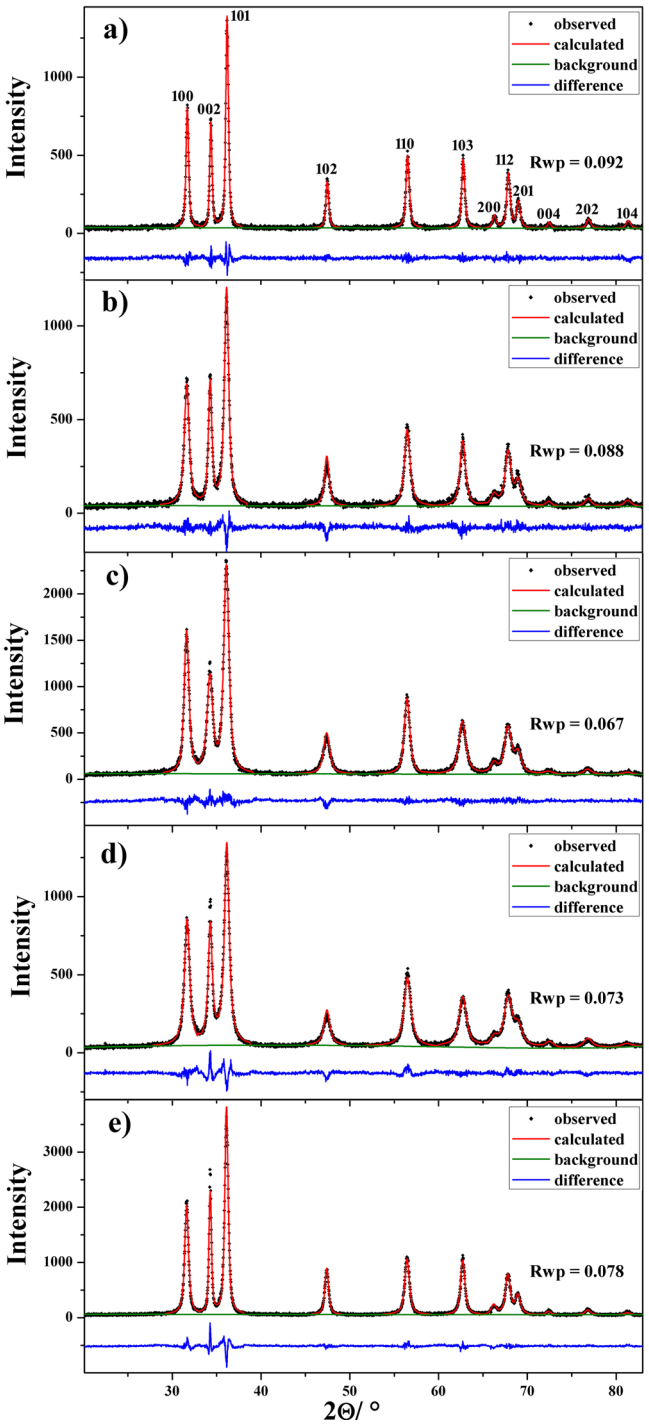

Figure 2. Results of Le Bail refinements on powder diffraction patterns of ZnO samples prepared at 170 °C for 4 h in (a) ethanol, (b) 1-propanol, (c) 1-butanol, (d) 1-pentanol, and (e) 1-octanol.

anisotropic ZnO nanorods with *c*-axis as the primary growth direction is susceptible to the type of solvents, having aspect ratios of 1.4, 1.4, 1.9, and 2.1 when ethanol, 1-propanol, 1-pentanol, and 1-octanol, respectively, was used (Table 1).

The obtained results indicate the presence of very small strains (parameters *Y*, *U*, and Y_e connected with the strain broadening converged toward zero). Values of the parameters connected with the size broadening (parameters *P*, *X*, and X_e) indicate, with the exception of sample obtained from 1-butanol, presence of size anisotropy with significantly bigger

Table 1. Estimated Values of the Volume-Averaged Domain Sizes (D_v) in the Direction Parallel (ϕ = 0°) and Perpendicular (ϕ = 90°) to the *c*-ax of Zincite Lattice As Determined from the Results of Le Bail Refinements (GSAS Program) on Powder Diffraction Patterns

sample	$D_v(\phi = 90°)$/nm	$D_v(\phi = 0°)$/nm	R_{wp}	aspect ratio
ethanol	28	40	0.092	1.4
1-propanol	14	19	0.088	1.4
1-butanol	12	12	0.067	1
1-pentanol	13	25	0.073	1.9
1-octanol	18	38	0.078	2.1

crystal growth in the direction parallel to *c*-axis compared to the directions perpendicular to *c*-axis. The results obtained by FE-SEM showed that in some alcoholic solvents ZnO nanoparticles aggregated in assembled spheres, whose sizes and morphologies depend on the type of alcohol used. The formation of ZnO nanorods which immediately thereafter assemble to form submicrometer spherical aggregates is especially favored in ethanol and 1-octanol, as shown in the SEM images of Figure 1, parts d and f. The characteristic thistle-like regular ZnO spheres up to 500 nm in size dominate in sample prepared in ethanol (Figure 1d), which seems less compact in comparison with spherical aggregates prepared in 1-octanol (Figure 1f). On the other hand, in the butanol solution, there was smaller tendency of aggregation of small spherical ZnO nanoparticles having approximately 10 times smaller size of uniform spherical ZnO aggregates than mentioned nanorods aggregates obtained in ethanol or 1-octanol (Figure 1e). Namely, in 1-butanol media, the final particles appear to be constituted by aggregation of a just few very fine spherical ZnO nanoparticles ~12 nm in size.

ZnO primary nanoparticles aggregated in assembled spheres (in ethanol and 1-octanol media) by means of noncovalent interactions such as hydrogen bonding, van der Waals forces, providing weaker or stronger electrostatic interaction depending on the type of alcohol used. The influence of alcohol on all steps, nucleation, and ZnO nanoparticle growth as well on the way of their aggregation is truly complex. The rod nanoparticles of ZnO showed a tendency to minimize surface energy by forming spherical aggregates with the lowest possible surface to volume ratio.

The Mechanism of ZnO Particle Formation. The solvothermal synthesis of ZnO nanoparticles involves two processes nucleation and growth. Generally, the formation of final ZnO particles can be divided into several sequential steps: (1) prenucleation intermediates formation, (2) nucleation, (3) crystal growth, and (4) possibly aggregation of ZnO nanoparticles. The presence of solvent molecules of different size and polarity had an significantly different influence on all of the processes, prenucleation, nucleation, crystal growth as well as on the possible aggregation of ZnO. Herein, the alcohol used acts as a solvent and reactant as well as controlling agent for particle growth. Small number of reactants during the solvothermal synthesis in pure alcohols allow studying of the chemical mechanism as well as control of reaction rates for all reaction steps involved in formation of final ZnO particles. The nucleation and growth mechanism of ZnO nanoparticles were investigated considering the results obtained by means of quantum chemical calculations at the density functional theory level (DFT). The experimental findings were corroborated by means of DFT calculations which were obtained by taking in

DOI: 10.1021/acs.jpcc.9b07411
J. Phys. Chem. C 2019, 123, 29394−29407

account effects of various alcoholic solvent, including ethanol, 1-propanol, 1-butanol, 1-pentanol, and 1-octanol. The DFT calculations revealed different binding affinities which initiated the processes of ZnO nucleation and growth in the presence of alcohols of different size and polarity, which could proceeded mainly through the reactions which involve different interactions such as van der Waals interactions, coordinate bonding, hydrogen bonding, screening effects, etc. Most probably, the synergistic effect of all the mentioned interactions is present. Thermodynamically, the nucleation and growth of final ZnO nanoparticles can be considered as a sequence of thermodynamic barriers which represent energy for prenucleation intermediates formation, nucleation and growth.

Prenucleation Intermediates Formation. ZnO−$CH_3(CH_2)_nOH$ ($n \leq 7$) species (monomer, dimer, etc.) can be considered as the prenucleation intermediate units which in the first step initiated the nucleation processes of ZnO nanoparticles. To initiate the nucleation process of ZnO a critical concentration of ZnO−$CH_3(CH_2)_nOH$ species in the solution is needed. Here, as a follow-up to our previous investigation[18] of the noncovalent interaction via O−H···O hydrogen bonding in ZnO−CH_3CH_2OH species (ethanol), we systematically studied and compared all the interactions involved in the processes of ZnO nucleation and growth in the presence of alcohols of different size and polarity, including ethanol, 1-propanol, 1-butanol, 1-pentanol, and 1-octanol. The calculated values of Gibbs free energies of ZnO−$CH_3(CH_2)_nOH$ ($n \leq 7$) molecular interactions (ΔG^*_{INT}) via O−H···O hydrogen bonding indicate an unusual order (ΔG^*_{INT} = −12.3 kcal mol^{-1} in ZnO−$CH_3(CH_2)_3OH$ (1-butanol); ΔG^*_{INT} = −11.51 kcal mol^{-1} in ZnO−CH_3CH_2OH (ethanol); ΔG^*_{INT} = −11.31 kcal mol^{-1} in ZnO−$CH_3(CH_2)_2OH$ (1-propanol); ΔG^*_{INT} = −10.4 kcal mol^{-1} in ZnO−$CH_3(CH_2)_4OH$ (1-pentanol); ΔG^*_{INT} = −9.42 kcal mol^{-1} in ZnO−$CH_3(CH_2)_7OH$ (1-octanol). If the hydrogen bonding was hypothetically the only factor, then the use of 1-butanol as solvent leads to more spontaneous formation of ZnO−$CH_3(CH_2)_nOH$ monomers and follow the unusual order 1-butanol > ethanol >1-propanol >1-pentanol >1-octanol. All the stable ZnO−$CH_3(CH_2)_nOH$ species, as well as calculated values of Gibbs free energies of interactions, where a binding was accomplished via a O−H···O hydrogen bonding are shown in Table S1, whereas bond lengths (d), energies (E), and QTAIM properties of the selected bonds in the monomers were summarized in Table S4). However, it is important to emphasize that the most stable ZnO−$CH_3(CH_2)_nOH$ monomers, where a binding was accomplished via a coordinate (Zn−O) bond, possess incomparably stronger coordination ability (shown in Figure 3a) which could replace weaker O−H···O hydrogen bonds (shown in Figure 3b). Namely, in the most stable conformation of the isolated ZnO−$CH_3(CH_2)_nOH$ monomer, the strongest binding was accomplished via a new coordinate bond, initiated with a characteristic ionic−dipolar interaction between hydrogen atoms from the alcohol hydroxyl group and oxygen in ZnO, which resulted in hydrogen atom transfer from the OH group on oxygen to ZnO. As a consequence of this process a lone electron pair on the oxygen atom from the alcohol hydroxyl group was involved in a new, significantly stronger coordinate bond with zinc (E_{Zn-O} ranges from −42.71 to −44.47 kcal mol^{-1}, as found in 1-butanol and 1-octanol media, shown in Table S4). The critical point of the Zn−O bond was characterized by the

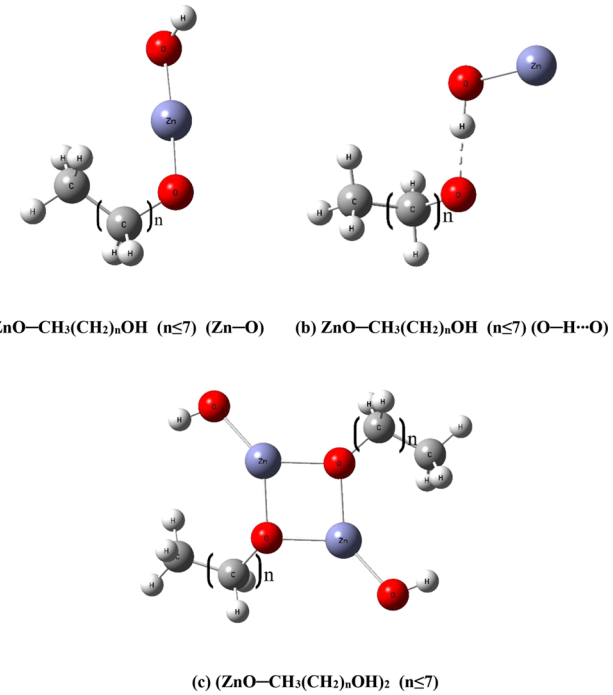

Figure 3. Most stable structures of ZnO−$CH_3(CH_2)_nOH$ monomers via selected bonds (a) coordinate (Zn−O) and (b) hydrogen (O−H···O) and (c) (ZnO−$CH_3(CH_2)_nOH)_2$ dimers in different alcohols, $CH_3(CH_2)_nOH$ (number of C atoms in hydrocarbon chain of alcohols, $n \leq 7$). The formation of (c) the most stable (ZnO−$CH_3(CH_2)_nOH)_2$ dimer from the association of most stable monomers in which the strongest binding was accomplished via coordinate (Zn−O) bonds. Red, blue, gray, and white spheres represent O, Zn, C and H atoms, respectively.

positive values of electron density Laplacian $\nabla^2\rho(r_c) > 0$ and by the negative value of electron energy density $H(r_c) < 0$ indicating this type of interaction as intermediate which is a feature of the coordinate bond, as shown in Table S4. When the mentioned coordinate bond, as the most important interaction responsible for stabilization in the ZnO−$CH_3(CH_2)_nOH$ species, was formed, the free energies of molecular interactions were released (ΔG^*_{INT} = −46.5 kcal mol^{-1} in ZnO−$CH_3(CH_2)_7OH$ (1-octanol); ΔG^*_{INT} = −44.1 kcal mol^{-1} in ZnO−$CH_3(CH_2)_4OH$ (1-pentanol); ΔG^*_{INT} = −43.5 kcal mol^{-1} in ZnO−$CH_3(CH_2)_3OH$ (1-butanol); ΔG^*_{INT} = −42.9 kcal mol^{-1} in ZnO−$CH_3(CH_2)_2OH$ (1-propanol); ΔG^*_{INT} = −42.04 kcal mol^{-1} in ZnO−CH_3CH_2OH (ethanol)). All the most stable ZnO−$CH_3(CH_2)_nOH$ species with the calculated values of Gibbs free energies of interactions are summarized in Table S1. It can be noticed that ZnO−$CH_3(CH_2)_nOH$ ($n \leq 7$) molecular interactions via a new coordinate bond increased the stability of the system yielding the especially stable ZnO−$CH_3(CH_2)_7OH$ (1-octanol) species, being, i.e., 4.46 kcal mol^{-1} more stable than the existing ZnO−CH_3CH_2OH (ethanol) monomer.

Alongside this, the formation of most stable dimer from the association of most stable monomers give evidence of coordinate bonding via free electron pair on oxygen atoms with zinc atoms and keep the same tetrahedral structural motif for the all most stable (ZnO−$CH_3(CH_2)_nO)_2$ dimers, having followed the values of Gibbs energies: ΔG^*_{INT} = −19.22 kcal mol^{-1} in (ZnO−$CH_3(CH_2)_7OH)_2$ (1-octanol); ΔG^*_{INT} =

DOI: 10.1021/acs.jpcc.9b07411
J. Phys. Chem. C 2019, 123, 29394−29407

-15.57 kcal mol^{-1} in $(ZnO-CH_3(CH_2)_4OH)_2$ (1-pentanol); $\Delta G^*_{INT} = -14.5$ kcal mol^{-1} in $(ZnO-CH_3(CH_2)_3OH)_2$ (1-butanol); $\Delta G^*_{INT} = -13.65$ kcal mol^{-1} in $(ZnO-CH_3(CH_2)_2OH)_2$ (1-propanol); $\Delta G^*_{INT} = -12.51$ kcal mol^{-1} in $(ZnO-CH_3CH_2OH)_2$ (ethanol) (Figure 3c, Table S1). It is important to emphasize that the formation of the most stable dimer (as shown in Figure 3c) from the optimal association of most stable monomers in which the strongest binding was accomplished via coordinate (Zn−O) bonds (Figure 3a) was studied.

Due to high chelating efficiency of alcohol molecules toward zinc, a same tetrahedral geometry which increased its stability was noticed in all $(ZnO-CH_3(CH_2)_nOH)_2$ dimers, as shown in Figure 3c. One can see that the use of nonpolar octanol as solvent leads also to more spontaneous formation $(ZnO-CH_3(CH_2)_7OH)_2$ (1-octanol) dimers than those obtained using polar shorter chain length alcohols being i.e. 6.1 kcal mol^{-1} more stable than the existing $(ZnO-CH_3CH_2OH)_2$ (ethanol) dimer. The calculated values of free energies of molecular interactions via the strongest coordinate bonding in both $ZnO-CH_3(CH_2)_nOH$ monomers as well as in $(ZnO-CH_3(CH_2)_nOH)_2$ dimers point out on a more spontaneous formation of such prenucleation intermediate with decreasing of the alcohol dielectric constant, in same order of 1-octanol >1-pentanol >1-butanol >1-propanol >1-ethanol. Furthermore, possible formation of other kinds of stable oligomers, i.e., the most stable tetramer of $(ZnO-CH_3(CH_2)_nOH)_4$, in all alcoholic solvent, from the association of two most stable $(ZnO-CH_3(CH_2)_nOH)_2$ dimers implies a species for which the formation process is also exergonic ($\Delta G^*_{INT} < 0$), and revealed also more spontaneous process for the longer-chain alcohols (as shown in Table S1).

The more or less spontaneous formation of the most stable $(ZnO-CH_3(CH_2)_nOH)_x$, $x \leq 4$, prenucleation intermediates in the presence of alcohols of different size and polarity plays a crucial role in the nucleation processes as a key step. However, it seems that more than one factor determinates the nucleation rate as well as ZnO crystal growth. The nuclei formation and preferential crystal growth present indeed a dynamic balance between solvent-sensitive processes of the prenucleation intermediates formation which initiate the nucleation of ZnO, the rate of growth of nuclei, and the dissolution process. The influence of alcohol environments on the nucleation and growth of ZnO nanoparticles was investigated in a series of alcohols from ethanol to 1-hexanol.[24,25] The authors emphasized that by changing the solvent from ethanol to 1-hexanol the nucleation process was significantly accelerated. Nucleation and growth are retarded in ethanol and 1-propanol compared to longer chain alcohols where nucleation and growth are fast. Alongside this, the solubility of the ZnO particles increases with increasing dielectric constant of the solvent.[24] The partially covalent nature of the bonding in ZnO is an important factor for determining the dissolution mechanism, i.e., for a purely ionic solid, the solubility could be expected to increase with increasing solvent dielectric constant. Sadasivan et al.[55] reported an alcoholic solvent effect on silica synthesis in a series of alcohols from ethanol to butanol. The rate of hydrolysis is fastest in 1-butanol and follow an unusual order of 1-butanol > methanol > ethanol >2-propanol >1-propanol. This is explained with two opposing factors that influenced the rate of hydrolysis, steric hindrance, and hydrogen bonding. It seems that the weaker hydrogen bonding between solvent molecules and nucleophile enhance the rate of hydrolysis, whereas the steric hindrance of an alkyl group expressed through higher solvent viscosity for higher alcohols reduces the rate of hydrolysis.[55] The authors concluded that the steric hindrance may be predominant factor for lower alcohols and weaker hydrogen bonding the predominant one for the higher alcohols. The authors concluded that the combination of these two factors is responsible for the unusual trend observed in the rate of hydrolysis.

Growth Process. The above-discussed results point to the formation mechanism of $(ZnO-CH_3(CH_2)_nOH)_x$, $x \leq 4$, prenucleation intermediates that initiated the nucleation processes of ZnO nanoparticles in various alcoholic solvents ($n \leq 7$), including ethanol, 1-propanol, 1-butanol, 1-pentanol, and 1-octanol. However, it was not possible to suggest mechanisms responsible for both the nucleation processes and preferential ZnO nanoparticles growth only from the knowledge of the most thermodynamically stable prenucleation intermediate units. Therefore, the theoretical study was extended to construction of small ZnO nanoclusters $(ZnO)_n$ (n = 12, 36),[35] to model the possible binding interactions involved in the processes of bare ZnO ultrasmall nanoparticles growth by taking in account effects of alcoholic solvents of different sizes and polarities. The prediction of the molecular geometries of small ZnO clusters has been the topic of a number of theoretical studies.[35,56] Chen et al.[35] constructed the $(ZnO)_n$ structures for $n \leq 168$ using a combined approach including structure discovery with genetic algorithms, density functional theory, and correlated molecular orbital theory at the coupled cluster (CCSD(T)) level. They reported the relation between electronic properties and particle sizes. They also found that the band gap of a spherical ZnO nanoparticle is predicted to be a linear function of the inverse of the particles diameter.

Alongside this, the small ZnO nanoclusters $(ZnO)_n$ (n = 12, 36) can serve as credible models for interface−solvent interactions in the present study. Possible binding sites on $(ZnO)_n$ clusters were calculated by DFT (shown in Table S5). So, the possible association of two small $(ZnO)_{12}$ clusters provide evidence of strong coordinate bonding via free electron pair on oxygen atoms with zinc atoms, having six possible binding sites, yielding the quite stable $(ZnO)_{24}$ structure as shown in Figure 4a with the following values of Gibbs energies: $\Delta G^*_{INT} = -69.16$ kcal mol^{-1} in octanol media; $\Delta G^*_{INT} = -67.12$ kcal mol^{-1} in 1-butanol; $\Delta G^*_{INT} = -66.1$ kcal mol^{-1} in 1-pentanol; $\Delta G^*_{INT} = -63.32$ kcal mol^{-1} in 1-propanol; $\Delta G^*_{INT} = -61.48$ kcal mol^{-1} in ethanol (Table S2). Interestingly, the calculated values of Gibbs free energies of interactions point out a more spontaneous connection of $(ZnO)_{12}-(ZnO)_{12}$ clusters following an unusual order of 1-octanol >1-butanol >1-pentanol >1-propanol > ethanol. The use of 1-octanol as an nonpolar media leads to a more spontaneous connection of $(ZnO)_{12}-(ZnO)_{12}$ clusters than those obtained using any polar alcohols in the series from ethanol to 1-penthanol. Furthermore, it is important to emphasize that changing the polar alcoholic solvent in the series from ethanol to 1-pentanol points out the most exergonic process in 1-butanol media. Similar tendency was also observed if the study was extended to the possible association of two $(ZnO)_{36}$ clusters, having ten possible coordinate Zn−O binding sites, yielding the quite stable $(ZnO)_{72}$ structure (Figure 4b), having followed the significantly higher values of Gibbs energies: $\Delta G^*_{INT} = -96.67$ kcal

DOI: 10.1021/acs.jpcc.9b07411
J. Phys. Chem. C 2019, 123, 29394−29407

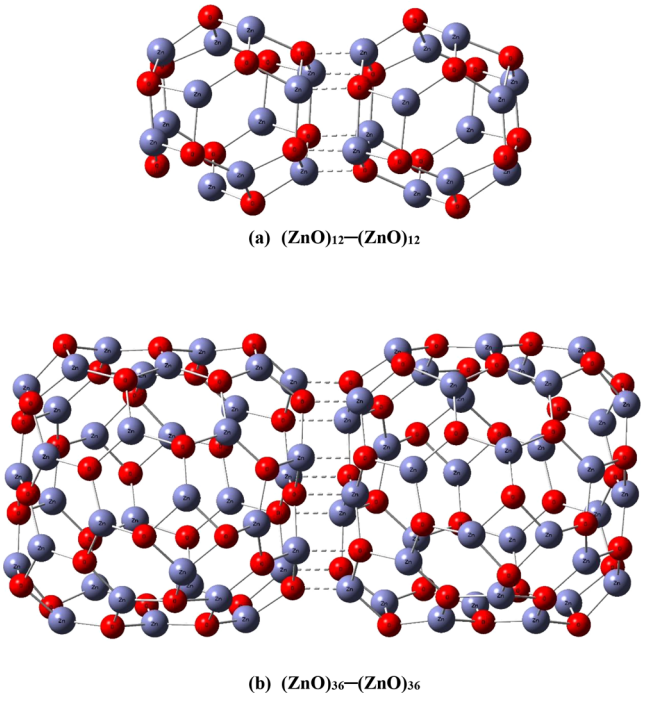

Figure 4. Most stable (a) $(ZnO)_{12}$–$(ZnO)_{12}$ and (b) $(ZnO)_{36}$–$(ZnO)_{36}$ structures. Red, blue, gray, and white spheres represent O, Zn, C, and H atoms, respectively.

mol^{-1} in octanol media; ΔG^*_{INT} = −95.35 kcal mol^{-1} in 1-butanol; ΔG^*_{INT} = −94.07 kcal mol^{-1} in 1-pentanol; ΔG^*_{INT} = −89.80 kcal mol^{-1} in 1-propanol; ΔG^*_{INT} = −74.82 kcal mol^{-1} in ethanol (Table S2). The calculations revealed the same unusual order of 1-octanol >1-butanol >1-pentanol >1-propanol > ethanol for the association of two $(ZnO)_{36}$ clusters as in the example of $(ZnO)_{12}$ clusters. The calculated values of the Gibbs free energy interactions obtained for spontaneous connection of both two $(ZnO)_{12}$, as well as two $(ZnO)_{36}$ clusters, suggested their high reactivity, as well as solvent sensitivity, providing a better insight into the mechanisms of ZnO crystal growth going from small clusters to ultrasmall nanoparticles to final nanoparticles. The advantages of association of two $(ZnO)_{36}$ clusters in nonpolar 1-octanol media should be emphasized in comparison to polar ethanol media, being 21.85 kcal mol^{-1} more stable.

Small nanoclusters reactivity in different media is probably key to understanding processes of ZnO nanoparticles growth or they represent the bridge between molecular clusters and the bare ZnO ultrasmall nanoparticles. ZnO in wurtzite structure is a typical polar crystal, whose polar axis is the *c*-axis. The formation of anisotropic ZnO nanorods with *c*-axis as the primary growth direction is susceptible to the type of solvents. The influence of the solvents on the nucleation and growth of ZnO nanoparticles have been reported by many researchers.[57−60] Tonto et al.[22] emphasized the interesting correlation between aspect ratio of ZnO nanorods and physical properties of the solvents in a series from 1-butanol to 1-decanol. The authors suggested that the interaction between the longer hydrocarbon chain alcohol molecules and slightly positive (001) facets of the ZnO crystal was weaker, allowing preferential ZnO crystal growth along the *c*-axis.[57−59] The preferred growth along the ZnO *c*-axis, or (001) direction, which related to both internal and external factors, is a typical behavior of ZnO. Generally, the overall crystal shape and the rate of crystal growth are determined by a combination of intrinsic crystal structure factors (intermolecular bonding preferences or dislocation in crystal) and external factors (supersaturation, temperature, type of solvent, impurities).[57−59] Cheng and Samulski[58] reported that the overall shape and growth rate of each face from ZnO crystals are also controlled by properties of solvent that affected the interface−solvent interactions. Zhang et al.[61] discussed the thermodynamic effect of three solvents with different polarity on the nucleus formation, preferential direction of crystal growth, and the amalgamation of crystals.

As a discussion of the FE SEM/XRD results of the present study (Structure and Morphology) shows, the use of 1-butanol as solvent leads to rather isotropic crystallite shape ($D_v \perp c$-ax ∼12 nm, ∼12, $D_v \| c$-ax ∼12 nm), revealed that each fine spherical ZnO nanoparticle consists of a single crystallite. The ZnO spherical nanoparticles were obtained only in the presence of 1-butanol, whereas in the presence of all remaining alcohols used ZnO nanoparticles grew prevailing in the *c*-direction to form nanorods. Indeed, the formation of anisotropic ZnO nanorods with *c*-axis as the primary growth direction is susceptible to the type of solvents, having aspect ratios of 1.4, 1.4, 1.9, and 2.1 when ethanol, 1-propanol, 1-pentanol, and 1-octanol, respectively, were used (Table 1). The absence of usual order in 1-butanol media indicates that more than one factor is determining the growth rate along its various face in different alcoholic solvent. The relative rates of crystal growth along its various faces, the aspect ratio, was influenced by reaction media as only major among all external factors in the present work. In summary, the results of X-ray diffraction size-strain analysis revealed that for the same experimental conditions in the presence of alcohols of different size and polarity, including ethanol, 1-propanol, 1-butanol, 1-pentanol, and 1-octanol, the relationships between the dielectric constant of alcoholic solvent and aspect ratio of crystals do not have consistency only in the presence of 1-butanol.

Interface−Solvent Interactions. Notwithstanding the parts of the formation mechanism that have been discussed above, a more detailed theoretical study of interface−solvent interactions is still needed to fully clarify preferential ZnO crystal growth in different reaction media.

The effects of alcoholic solvent on the overall shape and aspect ratio of ZnO crystals were investigated with detailed theoretical simulations of interface−solvent interactions by means of DFT calculations, which can be applied to justify the experimental findings.

It was verified by choosing a suitable model, i.e., the $(ZnO)_{12}$–$CH_3(CH_2)_nOH$, or $(ZnO)_{36}$–$CH_3(CH_2)_nOH$, $n \leq 7$, as theoretical hypothetical simulations of interface−solvent interactions by changing of alcoholic solvent from ethanol to 1-octanol. The calculations revealed different interface−solvent interactions which involve coordinate bonding, hydrogen bonding, van der Waals forces, electrostatic forces, etc. It seems very possible that the small $(ZnO)_{12}$ nanoclusters could be used to model $(ZnO)_{12}$–$CH_3(CH_2)_nOH$ binding interactions as theoretical simulations of interface−solvent interactions for ultrasmall nanoparticles in early stage of the growth, whereas $(ZnO)_{36}$ clusters could be used to model $(ZnO)_{36}$–$CH_3(CH_2)_nOH$ binding interactions as theoretical simulations of interface−solvent interactions for final ZnO nanoparticles.

DOI: 10.1021/acs.jpcc.9b07411
J. Phys. Chem. C 2019, 123, 29394−29407

If the small $(ZnO)_{12}$ cluster is used to model $(ZnO)_{12}$–$CH_3(CH_2)_nOH$ binding interactions (Figure 5a,b), the strongest binding was accomplished via an unusually short ($d_{O\cdots H}$ = 1.4 Å) and extremely strong O–H···O hydrogen bond between the hydrogen atom from a hydroxyl group of alcohol and oxygen in a $(ZnO)_{12}$ cluster (Figure 5b). The same atomic site in the $(ZnO)_{12}$ cluster has been chosen in all DFT calculations, which provide very accurate values of energies for all $(ZnO)_{12}$–$CH_3(CH_2)_nOH$ binding interactions (shown in Table S6). The calculated values of energies of a hydrogen bond are roughly close for all polar alcohols investigated in the series from ethanol to 1-pentanol, having close values of energies $E_{O\cdots H}$ ranging from −35.94 to −33.40 kcal mol^{-1}, whereas the energy is weaker for nonpolar octanol with $E_{O\cdots H}$ = −30.71 kcal mol^{-1} in $(ZnO)_{12}$–$CH_3(CH_2)_7OH$ (1-octanol) (Table S6). Also, there is another unusual occurrence of the less stable $(ZnO)_{12}$–$CH_3(CH_2)_nOH$ binding interactions accomplished via a coordinate bond between oxygen atoms from alcoholic hydroxyl group and zinc atoms in $(ZnO)_{12}$ cluster. Herein, $(ZnO)_{12}$–$CH_3(CH_2)_7OH$ (1-octanol) structure possess the strongest coordination ability with E_{Zn-O} = −19.43 kcal mol^{-1}, being, i.e., 2.21 kcal mol^{-1} stronger than the $(ZnO)_{12}$–CH_3CH_2OH (ethanol) structure (Table S6). This likely could be attributed to the fact that van der Waals forces are stronger in nonpolar longer-chain alcohol and could contribute to additional stabilization of the coordination bond, which was accomplished via a free electron pair on oxygen atoms from the hydroxyl group of alcohol and zinc atoms in the $(ZnO)_{12}$ cluster. Also, it is important to emphasize an unusual ability of the most stable conformation of $(ZnO)_{12}$–$CH_3(CH_2)_nOH$, which possessed about as twice as strong O–H···O hydrogen bonding ability ($E_{O\cdots H}$ ranges from −30.71 to 35.94 kcal mol^{-1}) than possible coordination Zn–O bonding ability (E_{Zn-O} ranges from −17.22 to 19.43 kcal mol^{-1}; Table S6). Moreover, when all is considered, from the calculated values of energies of bonding, which point to the unusual strength of hydrogen bond in comparison to coordination bond for $(ZnO)_{12}$–$CH_3(CH_2)_nOH$ and additional weaker van der Waals forces, as well as ΔG^*_{INT}, one might conclude that the presence of different alcoholic solvents was found to imply most important parameters by controlling the interface–solvent interactions allowing ultrasmall ZnO nanoparticles to grow or not only along the preferential *c*-axis. The results obtained by choosing of the $(ZnO)_{12}$–$CH_3(CH_2)_nOH$ model for simulation of interface–solvent interactions suggested that, due to weaker interaction of the longer-chain alcohols as octanol and polar a little positively charged Zn surface of ZnO crystal ($E_{O\cdots H}$ = −30.71 kcal mol^{-1}), the higher preferential growth rate along the *c*-axis was pronounced in comparison to polar alcoholic media (i.e., ethanol $E_{O\cdots H}$ = −35.94 kcal mol^{-1}). Tonto et al.[22] have reported a similar results for ZnO synthesized in various alcohols in a series from 1-butanol to 1-decanol. The authors emphasized that by changing the alcohol from 1-butanol to 1-decanol, the aspect ratio of ZnO nanorods increased from 1.7 to 5.6.

In a different manner, if the $(ZnO)_{36}$ nanocluster (diameters ∼1 nm) is used instead of $(ZnO)_{12}$ cluster to model $(ZnO)_{36}$–alcohol ($CH_3(CH_2)_nOH$) binding interactions as theoretical simulations of interface–solvent interactions, the calculations revealed special binding ability of $(ZnO)_{36}$ cluster to simultaneously participate in interactions common to both bonding types, coordination (Zn–O) and hydrogen (O–H···O) (Figure 6a,b). As a consequence of $(ZnO)_{36}$–$CH_3(CH_2)_nOH$ interaction, a lone electron pair on the oxygen atom from a hydroxyl group of alcohol was involved in a new coordinate bond with zinc (E_{Zn-O} ranges from −15.41 to −18.56 kcal mol^{-1}), which was supported by a extremely strong O–H···O hydrogen bonding interaction between the hydrogen atom from a that same hydroxyl group from alcohol and oxygen in $(ZnO)_{36}$ cluster ($E_{O\cdots H}$ ranges from −31.96 to −46.48 kcal mol^{-1}, Table S6). The calculated values of $E_{O\cdots H}$ (−31.96 kcal mol^{-1}) and E_{Zn-O} (E_{Zn-O} = −15.41 kcal mol^{-1}) of $(ZnO)_{36}$–$CH_3(CH_2)_7OH$ (1-octanol) interaction suggested that higher preferential growth rate along the *c*-axis was pronounced due to the weaker interaction of the nonpolar longer-chain alcohols such as 1-octanol with the polar and slightly positively charged Zn surface of the ZnO crystal in

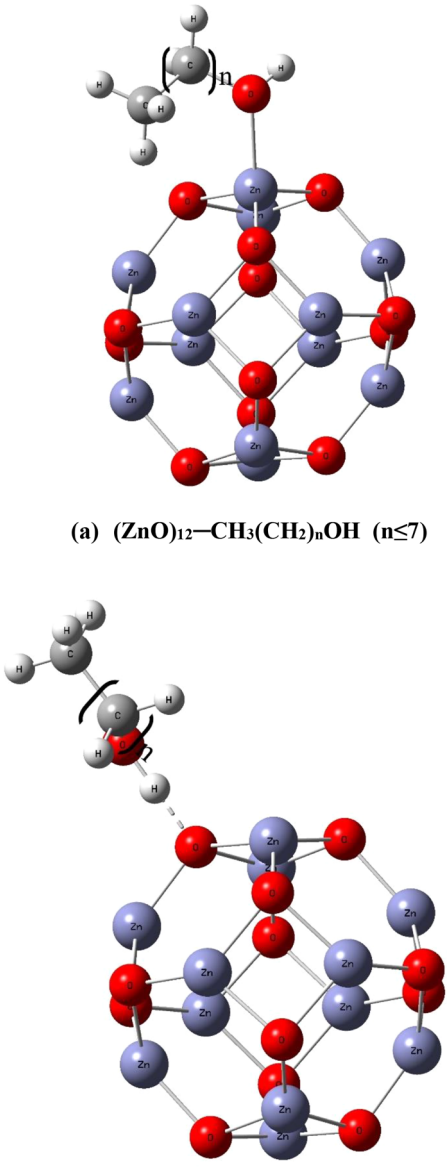

Figure 5. Most stable structures of $(ZnO)_{12}$–$CH_3(CH_2)_nOH$ via (a) coordinate (Zn–O) and (b) hydrogen (O–H···O) bonds in different alcohols (number of C atoms in hydrocarbon chain of alcohols, *n*). Red, blue, gray, and white spheres represent O, Zn, C, and H atoms, respectively.

DOI: 10.1021/acs.jpcc.9b07411
J. Phys. Chem. C 2019, 123, 29394–29407

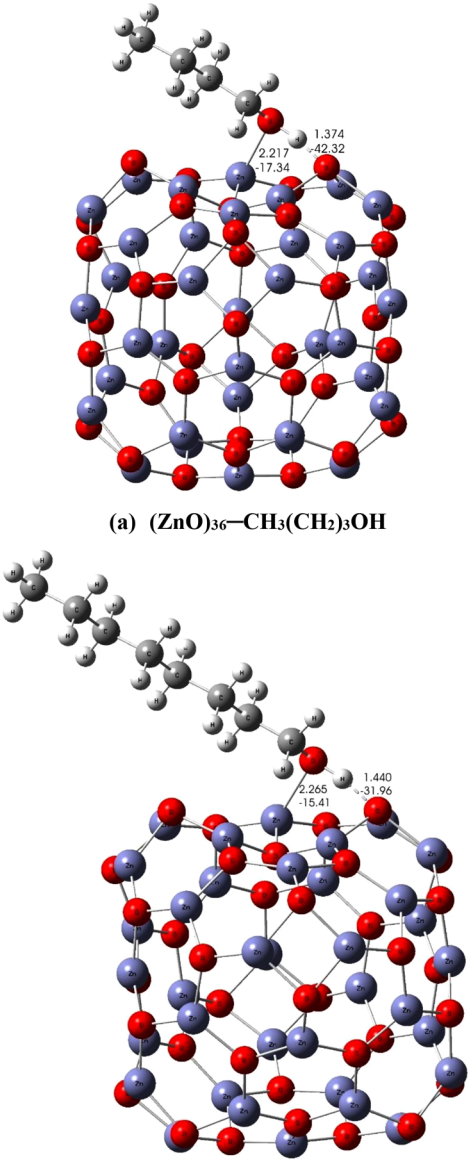

Figure 6. Most stable structures of (a) $(ZnO)_{36}$–$CH_3(CH_2)_3OH$ (1-butanol) and (b) $(ZnO)_{36}$–$CH_3(CH_2)_7OH$ (1-octanol) (selected values of bond distances in Å and bond energies in kcal mol^{-1}). Red, blue, gray, and white spheres represent O, Zn, C, and H atoms, respectively.

comparison to the interaction of polar alcoholic media ($E_{O\cdots H}$ = −46.48 kcal mol^{-1}; E_{Zn-O} = −18.56 kcal mol^{-1}, as found in ethanol media). Surprisingly, the most stable structure of $(ZnO)_{36}$–$CH_3(CH_2)_nOH$ ($n \leq 7$) possesses a more than twice as strong hydrogen bonding ability in comparison to coordination Zn−O bonding ability (Table S6). That difference in the results obtained by the DFT calculations of interface−solvent interactions by using $(ZnO)_{36}$ cluster instead smaller $(ZnO)_{12}$ is probably a consequence of the synergistic effect of the simultaneous involvement of both above-mentioned interactions, coordination as well as hydrogen bonding (Figure 6).

Therefore, it is important to emphasize that the $(ZnO)_{36}$–$CH_3(CH_2)_nOH$ ($n \leq 7$) interaction has been found to be a spontaneous exergonic process only in the presence of 1-butanol as reaction medium with ΔG^*_{INT} = −4.95 kcal mol^{-1}, whereas it is endergonic in the presence of all remaining alcohols used ($\Delta G^*_{INT} > 0$), (Table S3). Namely, the calculated Gibbs free energies of $(ZnO)_{36}$–$CH_3(CH_2)_nOH$ ($n \leq 7$) interaction revealed that the use of 1-butanol as solvent likely leads to a much stronger interface−solvent interaction in comparison to that for all the other alcohols used (Figure 6a), which finally results in nonpreferential crystal growth and spherical shape of ZnO nanoparticles only in 1-butanol media (according to XRD/FE SEM results, Figures 1 and 2 and Table S3). To sum up, the results obtained by the DFT calculations of interface−solvent interactions by using both model clusters $(ZnO)_n$ (n = 12 and 36), are in excellent agreement with the experimental microstructural study. Parts a and b of Figure 7 summarize both of the above-mentioned similar observations obtained in both experimental and theoretical studies, using known parameters, (a) diameter of ZnO crystallites or (b) Gibbs energy of $(ZnO)_{36}$–$CH_3(CH_2)_nOH$ interaction, both depending on the hydrocarbon chain length of alcohols, $n \leq 7$ $CH_3(CH_2)_nOH$.

The above-mentioned correlation of the results of calculated Gibbs free energies of the $(ZnO)_{36}$–$CH_3(CH_2)_nOH$ ($n \leq 7$) interaction (as theoretical simulations of interface−solvent interactions) with XRD/FE SEM results of the present study (Structure and Morphology) makes it possible to connect with general conclusion regarding the relative growth rate of ZnO along the preferential c-axis in different reaction media. It was established that the presence of 1-butanol as solvent had an unusually strong influence on the control of size of spherical ZnO nanoparticles just by interface−solvent interactions. Due to that reason, the use of 1-butanol as a solvent leads to spherical shape of ZnO nanoparticles, as well as crystallites smaller than those obtained in the presence of any other more or less polar alcohols investigated. It seems that it is not possible to predict mechanisms or bottleneck responsible for preferential growth of ZnO nanoparticles only from the knowledge obtained on the basis of the alcoholic solvent size and polarity. Generally, the overall shape and aspect ratio of ZnO is determined most probably by a combination of few opposing factors, structurally related internally, as well as the external effect of solvents.

Huang et al.[4] synthesized three kinds of ZnO nanoparticles with different facet exposures, including {0001} polar, {1011} semipolar, and {1010} nonpolar, by using a solvothermal method. Their results showed that the predominant facet of ZnO spherical nanoparticles was polar {0001} facets. The formation mechanism for different ZnO geometric structure and facet-dependent photocatalytic performance indicated dependence on the crystal facet exposures in the order {0001}> {10$\bar{1}$1} > {10$\bar{1}$0}. Hence, more interesting wurtzite 0001 surface have been extensively studied in a joint experimental and theoretical study.[35,62] Chen et al.[35] reported structural and electronic property study of $(ZnO)_n$ clusters and provide new insight in nucleation and crystallization processes of ZnO from small clusters to ultrasmall nanoparticles to regular nanoparticles. Their results showed that spherical zinc oxide nanoparticles will be predominately terminated by the wurtzite 0001 surface. Li et al.[63] was found that the crystal growth habit revealed the growth mechanism of the polar ZnO crystal and vice versa. The authors suggested that the {0001} facet of the crystal, which is slightly positively charged Zn surface, can be adsorbed by negatively charged chemical species and, consequently, retard the growth of the crystal in that direction.

DOI: 10.1021/acs.jpcc.9b07411
J. Phys. Chem. C 2019, 123, 29394−29407

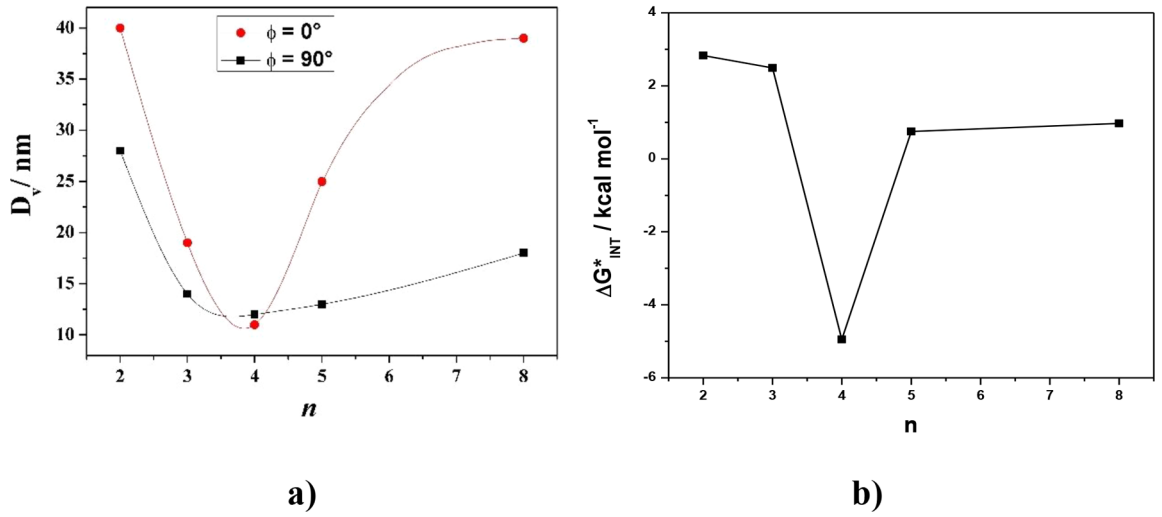

Figure 7. Correlation between diameter of ZnO crystallites ($D_v \perp c$-ax and $D_v \| c$-ax) (XRD) (a) or Gibbs energy of $(ZnO)_{36}-CH_3(CH_2)_nOH$ interaction, ΔG^*_{INT}, (DFT) (b) in dependence on the number of C atoms in hydrocarbon chain of different alcohols $CH_3(CH_2)_nOH$ ($n \leq 7$).

Furthermore, the ZnO nanoparticles obtained in ethanol and 1-octanol showed a tendency of spherical aggregation, as shown in the SEM images of Figure 1d,f. The growth mechanism of the ZnO spherical aggregates is of complex nature. The most important driving forces responsible for the growth mechanism of ZnO spherical aggregates, favored in ethanol and 1-octanol, are diverse interactions of the alcoholic solvent molecule with the surface of ZnO nanoparticles. Spherical aggregation of ZnO tiny particles is driven by means of noncovalent interactions such as hydrogen bonding, van der Waals forces, electrostatic forces, the screening effect, etc. The DFT calculations revealed different interface−solvent interactions in the presence of alcohols of different size and polarity. It is important to emphasize the impact of two types of bonds, strong O−H···O hydrogen bonds as dominant ones in ethanol and weaker van der Waals forces present as dominant ones in 1-octanol media, on the process of spherical aggregation of ZnO nanoparticles. The observed DFT results, such as calculated values of energies of hydrogen bond, provide evidence which implies that small polar molecules of ethanol were involved in the aggregation of ZnO nanoparticles via O−H···O hydrogen bonding, whereas long chain nonpolar molecules of 1-octanol could contribute to aggregation by weak van der Waals forces. Such noncovalent interactions could contribute even more to the compactness and stability of ZnO nanoparticle aggregates. Moreover, it seems that considerable spherical aggregate stability of final ZnO particles in ethanol media was achieved, whereas was lesser in 1-octanol media, according to FE SEM results (Figure 1d,f). It was corroborated by means of theoretical simulations of interface-solvent interaction by using both, $(ZnO)_{36}-CH_3(CH_2)_nOH$ as well as $(ZnO)_{12}-CH_3(CH_2)_nOH$ models. So, the calculated values of energies of a hydrogen bond, obtained by choosing of the $(ZnO)_{36}-CH_3CH_2OH$ (ethanol) model for interface−solvent interactions revealed that the use of ethanol as solvent likely leads to much stronger binding accomplished via O−H···O hydrogen bond with $E_{O\cdots H} = -46.48$ kcal mol^{-1}, whereas is weaker for nonpolar 1-octanol with $E_{O\cdots H} = -31.96$ kcal mol^{-1} in $(ZnO)_{36}-CH_3(CH_2)_7OH$ (1-octanol). A similar tendency was also observed for the $(ZnO)_{12}-CH_3(CH_2)_nOH$ model ($E_{O\cdots H} = -35.94$ kcal mol^{-1} in $(ZnO)_{12}-CH_3CH_2OH$ (ethanol), whereas $E_{O\cdots H} = -30.71$ kcal mol^{-1} in $(ZnO)_{12}-CH_3(CH_2)_7OH$ (1-octanol). The results of present study show a profound effect of surface interactions between the ZnO nanoparticles and alcohols of different size and polarity, i.e., ethanol and 1-octanol, on the mechanism of their aggregation.

4. CONCLUSIONS

In this research in a joint experimental and theoretical study, we presented the impact of five alcoholic reaction solvents including ethanol, 1-propanol, 1-butanol, 1-pentanol, and 1-octanol, on the nucleation and growth mechanism of ZnO nanoparticles. The reaction solvents of different sizes and polarities act as a solvent and reactant as well as control agents for particle growth, providing an significantly different influence on the all processes, nucleation, and crystal growth as well as on the possible aggregation of ZnO nanoparticles.

On the basis of the results of both microstructural and theoretical studies, the nucleation and preferential growth mechanism of ZnO nanoparticles is proposed. The results of both experimental and theoretical studies reveal that the nuclei formation and preferential crystal growth present indeed dynamic balance between solvent sensitive processes of the prenucleation intermediates formation which initiate the nucleation of ZnO and the rate of crystal growth. The DFT calculations revealed more spontaneous prenucleation intermediates formation for the longer-chain alcohols.

Different binding interactions involved in the processes of bare ZnO ultrasmall nanoparticle growth were established by possible association of small ZnO nanoclusters $(ZnO)_n$ (n = 12, 36), which served as credible models by taking in account effects of different alcoholic solvents. The calculated values of the Gibbs free energy interactions obtained for spontaneous association of $(ZnO)_n$ clusters, suggested their high reactivity as well as different solvent sensitivities. The advantages of association of two $(ZnO)_{36}$ clusters in nonpolar 1-octanol media should be emphasized in comparison to polar ethanol media, being 21.85 kcal mol^{-1} more stable.

Considering the results obtained from the theoretical simulations of interface−solvent interactions by using $(ZnO)_{36}-CH_3(CH_2)_nOH$ ($n \leq 7$) to model all the possible surface binding interactions involved between the formed ZnO nanoparticles and the molecules of alcoholic reaction solvents of different size and polarity, one might conclude that the

DOI: 10.1021/acs.jpcc.9b07411
J. Phys. Chem. C 2019, 123, 29394−29407

different growth rate along the preferential *c*-axis of polar ZnO crystal can be controlled mainly by the interface−alcohol interactions. It was established that the $(ZnO)_{36}$−$CH_3(CH_2)_nOH$ ($n \leq 7$) interaction is a spontaneous exergonic process only in the presence of 1-butanol as reaction medium with $\Delta G^*_{INT} = -4.95$ kcal mol^{-1}, whereas it is endergonic in the presence of all remaining alcohols used ($\Delta G^*_{INT} > 0$). The calculated value of the Gibbs free energy of $(ZnO)_{36}$−$CH_3(CH_2)_3OH$ (1-butanol) interaction revealed that the use of 1-butanol as alcoholic solvent leads to the strongest surface interaction in comparison to all other alcohols used, which finally results in nonpreferential crystal growth and spherical shape of ZnO nanoparticles only in 1-butanol media. It is interesting to note that the presence of 1-butanol as solvent had an unusually strong influence on the size control of spherical ZnO nanoparticles just by interface−solvent interactions. The observed results obtained by the DFT calculations of interface−solvent interactions are in excellent agreement with the XRD/FE SEM microstructural study. Indeed, the formation of anisotropic ZnO nanorods with *c*-axis as the primary growth direction is susceptible to the type of solvents, having aspect ratios of 1.4, 1.4, 1.9, and 2.1 when ethanol, 1-propanol, 1-pentanol, and 1-octanol, respectively, were used. It is interesting to note that the sole use of 1-butanol as solvent leads to a rather isotropic crystallite shape ($D_v \perp c$-ax ∼12, $D_v \| c$-ax ∼12 nm), whereas in the presence of all remaining alcohols ZnO nanoparticles grew prevailing in the *c*-direction to form nanorods. The absence of the usual order in 1-butanol media is indication that more than one factor is determining the growth rate along its various faces in different alcoholic solvents. The use of 1-butanol as a solvent leads to spherical shape of ZnO nanoparticles, as well as crystallites smaller than those obtained in the presence of any other more or less polar alcohols investigated.

It was established that the most stable structure of $(ZnO)_{36}$−$CH_3(CH_2)_nOH$ ($n \leq 7$) possesses more than twice as strong a hydrogen bonding ability in comparison to coordination Zn−O bonding ability. The calculated values of $(ZnO)_{36}$−$CH_3(CH_2)_7OH$ (1-octanol) interaction suggested that higher preferential growth rate along the *c*-axis was pronounced due to the weaker interaction of the nonpolar longer-chain alcohols as 1-octanol with polar and a small positively charged Zn surface of ZnO crystal in comparison to polar alcoholic media. It seems that it is not possible to predict mechanisms or bottlenecks responsible for preferential growth of ZnO nanoparticles only from the knowledge obtained on the basis of the alcoholic solvent size and polarity. One might concluded that the overall shape and preferential growth of ZnO nanoparticles is determined most probably by a combination of few opposing factors, structurally related internally, as well as external effect of solvents.

The results of the present research show the high impact of surface interactions between the obtained ZnO nanoparticles and the molecules of alcoholic reaction solvents of different size and polarity on the method of growth, which enables a good control of their morphological properties.

■ ASSOCIATED CONTENT

Supporting Information

The Supporting Information is available free of charge on the ACS Publications website at DOI: 10.1021/acs.jpcc.9b07411.

Optimized structures of all investigated species, tables of interaction Gibbs free energies, QTAIM parameters, data of energies (E^{Tot}_{soln}, $\Delta G^*_{VRT,soln}$, G^*_X), and optimized Cartesian atomic coordinates (PDF)

■ AUTHOR INFORMATION

Corresponding Author

*Telephone: +385 1 45 61 111. Fax: +385 1 46 80 098 E-mail: Ankica.Saric@irb.hr (A.Š.).

ORCID

Ankica Šarić: 0000-0002-3211-2360

Notes

The authors declare no competing financial interest.

■ ACKNOWLEDGMENTS

The authors thank mag.ing.arch. Marin Josipović for help with graphic expression. This work has been partially supported by SAFU, Project KK.01.1.1.01.0001. The authors would like to thank the Zagreb University Computing Centre (SRCE) for generously granting computational resources on the ISABELLA cluster (isabella.srce.hr).

■ REFERENCES

(1) Pearton, S. J.; Norton, D. P.; Ip, K.; Heo, Y. W.; Steiner, T. Recent Progress in Processing and Properties of ZnO. *Prog. Mater. Sci.* **2005**, *50*, 293−340.

(2) Ozgur, U.; Alivov, Ya. I.; Liu, C.; Teke, A.; Reshchikov, M. A.; Dogan, S.; Avrutin, V.; Cho, S.-J.; Morkoc, H. A Comprehensive Review of ZnO Materials and Devices. *J. Appl. Phys.* **2005**, *98*, 041301.

(3) Hoffmann, M. R.; Martin, S. T.; Choi, W.; Bahnemann, D. W. Environmental Applications of Semiconductor Photocatalysis. *Chem. Rev.* **1995**, *95*, 69−96.

(4) Huang, M.; Weng, S.; Wang, B.; Hu, J.; Fu, X.; Liu, P. Various Facet Tunable ZnO Crystals by a Scalable Solvothermal Synthesis and Their Facet-Dependent Photocatalytic Activities. *J. Phys. Chem. C* **2014**, *118*, 25434−25440.

(5) Boppella, R.; Anjaneyulu, K.; Basak, P.; Manorama, S. V. Facile Synthesis of Face Oriented ZnO Crystals: Tunable Polar Facets and Shape Induced Enhanced Photocatalytic Performance. *J. Phys. Chem. C* **2013**, *117*, 4597−4605.

(6) Alenezi, M. R.; Alshammari, A. S.; Jayawardena, K. D. G. I.; Beliatis, M. J.; Henley, S. J.; Silva, S. R. P. Role of the Exposed Polar Facets in the Performance of Thermally and UV Activated ZnO Nanostructured Gas Sensors. *J. Phys. Chem. C* **2013**, *117*, 17850−17858.

(7) Xiao, Y.; Lu, L.; Zhang, A.; Zhang, Y.; Sun, L.; Huo, L.; Li, F. Highly Enhanced Acetone Sensing Performances of Porous and Single Crystalline ZnO Nanosheets: High Percentage of Exposed (100) Facets Working Together with Surface Modification with Pd Nanoparticles. *ACS Appl. Mater. Interfaces* **2012**, *4*, 3797−3804.

(8) Zhang, Z.; Wang, S. J.; Yu, T.; Wu, T. Controlling the Growth Mechanism of ZnO Nanowires by Selecting Catalysts. *J. Phys. Chem. C* **2007**, *111*, 17500−17505.

(9) Xu, L.; Hu, Y.-L.; Pelligra, C.; Chen, C.-H.; Jin, L.; Huang, H.; Sithambaram, S.; Aindow, M.; Joesten, R.; Suib, S. L. ZnO with Different Morphologies Synthesized by Solvothermal Methods for Enhanced Photocatalytic Activity. *Chem. Mater.* **2009**, *21*, 2875−2885.

(10) Chaudhari, R.; Landge, D.; Bhongale, C. J. A New Insight Into the Adsorption−Dissolution Growth Mechanism of Zinc Oxide Hollow Hexagonal Nanotowers. *RSC Adv.* **2019**, *9*, 20728−20732.

(11) Ludi, B.; Niederberger, M. Zinc Oxide Nanoparticles: Chemical Mechanisms and Classical and Non-Classical Crystallization. *Dalton Trans.* **2013**, *42*, 12554−12568.

(12) Musić, S.; Šarić, A. Formation of Hollow ZnO Particles by Simple Hydrolysis of Zinc Acetylacetonate. *Ceram. Int.* **2012**, *38*, 6047−6052.
(13) Salavati-Niasari, M.; Davar, F.; Khansari, A. Nanospherical and Nanobundles of ZnO: Synthesis and Characterization. *J. Alloys Compd.* **2011**, *509*, 61−65.
(14) Mir, N.; Salavati-Niasari, M.; Davar, F. Preparation of ZnO Nanoflowers and Zn Glycerolate Nanoplates Using Inorganic Precursors via a Convenient Rout and Application in Dye Sensitized Solar Cells. *Chem. Eng. J.* **2012**, *181*−*182*, 779−789.
(15) Anžlovar, A.; Kogej, K.; Orel, Z. C.; Žigon, M. Impact of Inorganic Hydroxides on ZnO Nanoparticle Formation and Morphology. *Cryst. Growth Des.* **2014**, *14*, 4262−4269.
(16) Wojnarowicz, J.; Chudoba, T.; Koltsov, I.; Gierlotka, S.; Dworakowska, S.; Lojkowski, W. Size Control Mechanism of ZnO Nanoparticles Obtained in Microwave Solvothermal Synthesis. *Nanotechnology* **2018**, *29*, 065601−065623.
(17) Šarić, A.; Štefanić, G.; Dražić, G.; Gotić, M. Solvothermal Synthesis of Zinc Oxide Microspheres. *J. Alloys Compd.* **2015**, *652*, 91−99.
(18) Šarić, A.; Despotović, I.; Štefanić, G.; Dražić, G. The Influence of Ethanolamines on the Solvothermal Synthesis of Zinc Oxide: A Combined Experimental and Theoretical Study. *ChemistrySelect* **2017**, *2*, 10038−10049.
(19) Šarić, A.; Despotović, I.; Štefanić, G. Solvothermal Synthesis of Zinc Oxide Nanoparticles: A Combined Experimental and Theoretical Study. *J. Mol. Struct.* **2019**, *1178*, 251−260.
(20) Inubushi, Y.; Takami, R.; Iwasaki, M.; Tada, H.; Ito, S. Mechanism of Formation of Nanocrystalline ZnO Particles through the Reaction of [Zn(Acac)2] with NaOH in EtOH. *J. Colloid Interface Sci.* **1998**, *200*, 220−227.
(21) Du, H.; Yuan, F.; Huang, S.; Li, J.; Zhu, Y. A New Reaction to ZnO Nanoparticles. *Chem. Lett.* **2004**, *33*, 770−771.
(22) Tonto, P.; Mekasuwandumrong, O.; Phatanasri, S.; Pavarajarn, V.; Praserthdam, P. Preparation of ZnO Nanorod by Solvothermal Reaction of Zinc Acetate in Various Alcohols. *Ceram. Int.* **2008**, *34*, 57−62.
(23) Šarić, A.; Gotić, M.; Štefanić, G.; Dražić, G. Synthesis of ZnO Particles Using Water Molecules Generated in Esterification Reaction. *J. Mol. Struct.* **2017**, *1140*, 12−18.
(24) Hu, Z.; Oskam, G.; Searson, P. C. Influence of Solvent on the Growth of ZnO Nanoparticles. *J. Colloid Interface Sci.* **2003**, *263*, 454−460.
(25) Oskam, G.; Poot, F. de J. P. Synthesis of ZnO and TiO2 Nanoparticles. *J. Sol-Gel Sci. Technol.* **2006**, *37*, 157−160.
(26) Niederberger, M. Nonaqueous Sol−Gel Routes to Metal Oxide Nanoparticles. *Acc. Chem. Res.* **2007**, *40*, 793−800.
(27) Pinna, N.; Niederberger, M. Surfactant-Free Nonaqueous Synthesis of Metal Oxide Nanostructures. *Angew. Chem., Int. Ed.* **2008**, *47*, 5292−5304.
(28) Le Bail, A.; Duroy, H.; Fourquet, J. L. Ab-Initio Structure Determination of LiSbWO6 by X-Ray Powder Diffraction. *Mater. Res. Bull.* **1988**, *23*, 447−452.
(29) Larson, A. C.; Von Dreele, R. B. General Structure Analysis System GSAS; *Los Alamos National Laboratory Report*, 2001.
(30) Toby, B. H. *EXPGUI*, a Graphical User Interface for *GSAS*. *J. Appl. Crystallogr.* **2001**, *34*, 210−213.
(31) Balzar, D.; Audebrand, N.; Daymond, M. R.; Fitch, A.; Hewat, A.; Langford, J. I.; Le Bail, A.; Louër, D.; Masson, O.; McCowan, C. N.; et al. Size−strain Line-Broadening Analysis of the Ceria Round-Robin Sample. *J. Appl. Crystallogr.* **2004**, *37*, 911−924.
(32) Thompson, P.; Cox, D. E.; Hastings, J. B. Rietveld Refinement of Debye−Scherrer Synchrotron X-Ray Data from Al_2O_3. *J. Appl. Crystallogr.* **1987**, *20*, 79−83.
(33) Štefanić, G.; Krehula, S.; Štefanić, I. The High Impact of a Milling Atmosphere on Steel Contamination. *Chem. Commun.* **2013**, *49*, 9245−9247.
(34) Frisch, M. J.; Trucks, G. W.; Schlegel, H. B.; Scuseria, G. E.; Robb, M. A.; Cheeseman, J. R.; Scalmani, G.; Barone, V.; Mennucci, B.; Petersson, G. A. et al. *Gaussian 09*, Revision D.01; Gaussian, Inc.: Wallingford, CT, 2009.
(35) Chen, M.; Straatsma, T. P.; Fang, Z.; Dixon, D. A. Structural and Electronic Property Study of (ZnO)n, $n \leq 168$: Transition from Zinc Oxide Molecular Clusters to Ultrasmall Nanoparticles. *J. Phys. Chem. C* **2016**, *120*, 20400−20418.
(36) Zhao, Y.; Schultz, N. E.; Truhlar, D. G. Design of Density Functionals by Combining the Method of Constraint Satisfaction with Parametrization for Thermochemistry, Thermochemical Kinetics, and Noncovalent Interactions. *J. Chem. Theory Comput.* **2006**, *2*, 364−382.
(37) Zhao, Y.; Truhlar, D. G. Density Functionals with Broad Applicability in Chemistry. *Acc. Chem. Res.* **2008**, *41*, 157−167.
(38) Zhao, Y.; Truhlar, D. G. Density Functional Theory for Reaction Energies: Test of Meta and Hybrid Meta Functionals, Range-Separated Functionals, and Other High-Performance Functionals. *J. Chem. Theory Comput.* **2011**, *7*, 669−676.
(39) Amin, E. A.; Truhlar, D. G. Zn Coordination Chemistry: Development of Benchmark Suites for Geometries, Dipole Moments, and Bond Dissociation Energies and Their Use to Test and Validate Density Functionals and Molecular Orbital Theory. *J. Chem. Theory Comput.* **2008**, *4*, 75−85.
(40) Cramer, C. J.; Truhlar, D. G. Density Functional Theory for Transition Metals and Transition Metal Chemistry. *Phys. Chem. Chem. Phys.* **2009**, *11*, 10757−10816.
(41) Hay, P. J.; Wadt, W. R. *Ab Initio* Effective Core Potentials for Molecular Calculations. Potentials for the Transition Metal Atoms Sc to Hg. *J. Chem. Phys.* **1985**, *82*, 270−283.
(42) Marenich, A. V.; Cramer, C. J.; Truhlar, D. G. Universal Solvation Model Based on the Solvent Defined by the Bulk Dielectric Constant and Atomic Surface Tensions. *J. Phys. Chem. B* **2009**, *113*, 6378−6396.
(43) Bader, R. F. W. *Atoms in Molecules: a Quantum Theory*; Clarendon Press: Oxford, U.K., 1990.
(44) Keith, T. A. *AIMAll (Version 17.01.25)*; TK Gristmill Software: Overland Park KS, 2017.
(45) Bader, R. F. W. A Bond Path: a Universal Indicator of Bonded Interactions. *J. Phys. Chem. A* **1998**, *102*, 7314−7323.
(46) Bader, R. F. W.; Essen, H. The Characterization of Atomic Interactions. *J. Chem. Phys.* **1984**, *80*, 1943−1960.
(47) Cremer, D.; Kraka, E. A Description of the Chemical Bond in Terms of Local Properties of Electron Density and Energy. *Croat. Chem. Acta* **1984**, *57*, 1259−1281.
(48) Espinosa, E.; Molins, E.; Lecomte, E. Hydrogen Bond Strengths Revealed by Topological Analyses of Experimentally Observed Electron Densities. *Chem. Phys. Lett.* **1998**, *285*, 170−173.
(49) Espinosa, E.; Alkorta, I.; Rozas, I.; et al. About the Evaluation of the Local Kinetic, Potential and Total Energy Densities in Closed-shell Interactions. *Chem. Phys. Lett.* **2001**, *336*, 457−461.
(50) Borissova, A. O.; Antipin, M. Yu.; Karapetyan, H. A.; Petrosyan, A. M.; Lyssenko, K. A. Cooperativity Effects of H-Bonding and Charge Transfer in an L-Nitroarginine Crystal with $Z' > 1$. *Mendeleev Commun.* **2010**, *20*, 260−262.
(51) Baryshnikov, G. V.; Minaev, B. F.; Minaeva, V. A.; Nenajdenko, V. G. Single Crystal Architecture and Absorption Spectra of Octathio[8]circulene and *Sym*-tetraselenatetetrathio[8]circulene: QTAIM and TD-DFT Approach. *J. Mol. Model.* **2013**, *19*, 4511−4519.
(52) Baryshnikov, G. V.; Minaev, B. F.; Korop, A. A.; Minaeva, V. A.; Gusev, A. N. Structure of Zinc Complexes with 3-(Pyridin-2-yl)-5-(arylideneiminophenyl)-1*H*-1,2,4-triazoles in Different Tautomeric Forms: DFT and QTAIM Study. *Russ. J. Inorg. Chem.* **2013**, *58*, 928−934.
(53) Shahangi, F.; Chermahini, A. N.; Farrokhpour, H.; Teimouri, A. Selective Complexation of Alkaline Earth Metal Ions with Nanotubular Cyclopeptides: DFT Theoretical Study. *RSC Adv.* **2015**, *5*, 2305−2317.
(54) Puntus, L. N.; Lyssenko, K. A.; Antipin, M. Yu.; Bünzli, J.-C. G. Role of Inner- and Outer-Sphere in the Sensitization of Eu^{III}-Luminescence Deciphered by Combined Analysis of Experimental

DOI: 10.1021/acs.jpcc.9b07411
J. Phys. Chem. C 2019, 123, 29394−29407

Electron Density Distribution Function and Photophysical Data. *Inorg. Chem.* **2008**, *47*, 11095−11107.
(55) Sadasivan, S.; Dubey, A. K.; Li, Y.; Rasmussen, D. H. Alcoholic Solvent Effect on Silica Synthesis—NMR and DLS Investigation. *J. Sol-Gel Sci. Technol.* **1998**, *12*, 5−14.
(56) Zhao, M.; Xia, Y.; Tan, Z.; Liu, X.; Mei, L. Design and Energetic Characterization of ZnO Clusters from First-Principles Calculations. *Phys. Lett. A* **2007**, *372*, 39−43.
(57) Cheng, B.; Samulski, E. T. Hydrothermal Synthesis of One-Dimensional ZnO Nanostructures with Different Aspect Ratios. *Chem. Commun.* **2004**, *8*, 986−987.
(58) Cheng, B.; Shi, W.; Russell-Tanner, J. M.; Zhang, L.; Samulski, E. T. Synthesis of Variable-Aspect-Ratio, Single-Crystalline ZnO Nanostructures. *Inorg. Chem.* **2006**, *45*, 1208−1214.
(59) Kunjara Na Ayudhya, S.; Tonto, P.; Mekasuwandumrong, O.; Pavarajarn, V.; Praserthdam, P. Solvothermal Synthesis of ZnO with Various Aspect Ratios Using Organic Solvents. *Cryst. Growth Des.* **2006**, *6*, 2446−2450.
(60) Ambrožič, G.; Škapin, S. D.; Žigon, M.; Orel, Z. C. The Synthesis of Zinc Oxide Nanoparticles from Zinc Acetylacetonate Hydrate and 1-Butanol or Isobutanol. *J. Colloid Interface Sci.* **2010**, *346*, 317−323.
(61) Zhang, J.; Sun; Yin; Su; Liao; Yan. Control of ZnO Morphology via a Simple Solution Route. *Chem. Mater.* **2002**, *14*, 4172−4177.
(62) Irani, M.; Mohammadi, T.; Mohebbi, S. Photocatalytic Degradation of Methylene Blue with ZnO Nanoparticles; a Joint Experimental and Theoretical Study. *J. Mex. Chem. Soc.* **2017**, *60*, 218−225.
(63) Li, W.-J.; Shi, E.-W.; Zhong, W.-Z.; Yin, Z.-W. Growth Mechanism and Growth Habit of Oxide Crystals. *J. Cryst. Growth* **1999**, *203*, 186−196.

DOI: 10.1021/acs.jpcc.9b07411
J. Phys. Chem. C 2019, 123, 29394−29407